PAPER

Surface micromachined electrostatically actuated micro peristaltic pump

Jun Xie,*[a] Jason Shih,[a] Qiao Lin,[b] Bozhi Yang[b] and Yu-Chong Tai[a]

[a] *Department of Electrical Engineering, California Institute of Technology, Pasadena, CA, 91125, USA. E-mail: junxie@mems.caltech.edu; Fax: 626-584-9104; Tel: 626-395-2254*

[b] *Department of Mechanical Engineering, Carnegie Mellon University, Pittsburgh, PA, 15213, USA. E-mail: qlin@andrew.cmu.edu; Fax: 412-268-3348; Tel: 412-268-3641*

Received 15th March 2004, Accepted 8th June 2004
First published as an Advance Article on the web 14th September 2004

An electrostatically actuated micro peristaltic pump is reported. The micro pump is entirely surface micromachined using a multilayer parylene technology. Taking advantage of the multilayer technology, the micro pump design enables the pumped fluid to be isolated from the electric field. Electrostatic actuation of the parylene membrane using both DC and AC voltages was demonstrated and applied to fluid pumping based on a 3-phase peristaltic sequence. A maximum flow rate of 1.7 nL min^{-1} and an estimated pumping pressure of 1.6 kPa were achieved at 20 Hz phase frequency. A dynamic analysis was also performed with a lumped-parameter model for the peristaltic pump. The analysis results allow a quantitative understanding of the peristaltic pumping operation, and correctly predict the trends exhibited by the experimental data. The small footprint of the micro pump is well suited for large-scale integration of microfluidics. Moreover, because the same platform technology has also been used to fabricate other devices (*e.g.* valves, electrospray ionization nozzles, filters and flow sensors), the integration of these different devices can potentially lead to versatile and functional micro total analysis systems (μTAS).

Introduction

Recently there has been enormous interest in the research and development of microfluidics because of increasing demands from biological applications such as genomics,[1] proteomics,[2] and drug discovery. The micro pump is one of the most important microfluidic devices for μTAS. It provides the driving force to mobilize fluids in the system, which then enables functions such as mixing, reaction, injection, and separation. Previously, micro pumps have been demonstrated using several actuation mechanisms and fabrication technologies.[3] Unfortunately, most of them have inherent technological limitations that prevent their use in large-scale integration.

In general, pumps can be divided into two categories: mechanical pumps and non-mechanical pumps. Because non-mechanical pumps can be realized using simple structures without moving parts, they are straightforward in terms of fabrication and well suited for integration. However, their performance often critically depends on fluid and surface properties. For example, electroosmotic pumping can be affected by such properties as permittivity and zeta potential.[4] Similarly, electrohydrodynamic pumps are directly affected by the conductivity of the fluid.[5] Also, fluid transport based on electrowetting is highly dependent on the fluid's surface tension.

Mechanical pumps can handle a large variety of fluids, but often involve complicated structures and present integration challenges, as is evident in rotary pumps (requiring bearings) and some diaphragm pumps (requiring check valves). However, peristaltic pumps are a class of mechanical pumps that are relatively simple in structure and suitable for miniaturization. Moreover, electrostatic actuation is well suited to peristaltic pumping. It consumes much less power than other actuation mechanisms (*e.g.*, thermopneumatic actuation) while still delivering reasonable pumping flow rates and pressures. Compared to piezoelectric actuation, electrostatic actuation can produce more displacement without complicated fabrication, leading to a higher expansion/compression ratio. Since microfluidic systems are especially useful for biological applications, the low-power and low-temperature operation of electrostatic pumping is even more attractive. Despite these advantages, electrostatic pumping has not been adequately investigated in the literature. An electrostatic pump using plastic molding technology was reported but offered only limited miniaturization.[6] Another micromachined electrostatic peristaltic pump was reported without any testing results.[7] We report here the first completely surface-micromachined and electrostatically actuated peristaltic pump, and demonstrate its successful operation. In addition, we present a lumped-parameter model to analyze the operation of the peristaltic pump. With the model, the dynamics of peristaltic pumping, not addressed by existing micro pump models,[8–10] are appropriately investigated. We consider the dynamics of individual pumping chambers and account for the interactions of such component dynamics by a system representation of the peristaltic pump. The resulting model can quantitatively explain important pumping characteristics such as flow rate and pumping pressure, and correctly predict the trend in the experimentally observed pump characteristics.

The micro pump is realized by a multilayer parylene, surface-micromachining technology that we have recently developed[11] to enable large-scale microfluidics. Similar approaches to polymer-based microfluidic integration have also been reported by other researchers. For example, a multilayer PDMS microfluidic system was developed that allows rapid prototyping[12] and large-scale integration.[13] However, this type of system still requires off-chip pneumatic supply and control, which could potentially limit the miniaturization of the whole system and its application in portable systems. The motivation for the development of our multilayer parylene technology is to enable the integration of various fluidic devices on a single chip. By using a common fabrication technology for all devices, the difficulty of integrating multiple devices, which are fabricated using different technologies, is eliminated. Moreover, the integration on a single chip also eliminates problems (*e.g.*,

DOI: 10.1039/b403906h

precise alignment and micro plumbing) encountered in multi-chip packaging.

Design and fabrication

Design

A schematic of the mechanical structure and operation principle of the micro pump is given by Fig. 1. Because the micro pump is based on surface-micromachining technology, its basic design is chosen to be a membrane pump. It has three pumping chambers connected in series. Essential components of each pumping chamber include an actuation chamber, a fluid channel, and a moving membrane that separates them. The actuation chamber is vented to the ambient through a venting hole. A fixed ground electrode is located on the substrate at the bottom of the actuation chamber and coated with parylene to isolate it from the environment. A top electrode is incorporated into the moving membrane and is sandwiched between two parylene layers. Together, this composite structure forms the moving membrane. On top of the moving membrane, the fluid channel is created which runs through all three pumping chambers. When an actuation voltage is applied between the two electrodes, electrostatic force will pull down the membrane and cause volume expansion in the fluid channel on top. When the three pumping chambers are actuated using a 3-phase peristaltic sequence,[14] the resulting peristaltic motion will induce pumping of the fluid inside the channel. A key feature of this design is that the electric field is confined inside the actuation chamber, which is filled with air, so it is separated from the liquid-filled fluid channel. Previously reported pumps[7] lacked this feature. This key advantage is made possible by the multilayer technology. This pump design greatly reduces the risk of electrolysis inside the fluid channel, and is also highly desirable for applications involving biological substances or chemical reagents, such as proteins and cells, which could be affected by high electric fields.

Electrostatic pull-in is a well-known instability in the behavior of an elastically supported parallel-plate electrostatic actuator. To achieve maximum volume compression/expansion ratio, the pump needs to operate around the pull-in mode so the membrane deflection can be at a maximum. We adopted a closed-form model[15] for the pull-in voltage of clamped circular diaphragms, which is approximately the case for the moving membrane. The model accounts for contributions of both bending stiffness and residual membrane stress to the overall membrane stiffness, and takes the form

$$V_P = \sqrt{\frac{1.55\sigma t_m (d + t_i/\varepsilon_p)^3}{\alpha \varepsilon_0 r^2}} \quad (1)$$

where $\alpha = 1 + 2(1 - \cosh \kappa)/(\kappa \sinh \kappa)$ and $\kappa = 0.825 (r/t_m)[12(1 - v^2)\sigma/E]^{1/2}$. Here σ, E and v are the residual stress, Young's modulus, and Poisson's ratio of parylene. r and t_m are the membrane radius and thickness, d is the initial electrode gap height, t_i and ε_p are the thickness and dielectric constant of the parylene insulation layers between the electrodes, and ε_0 is the perimittivity of free space. These symbols are also listed in the Appendix.

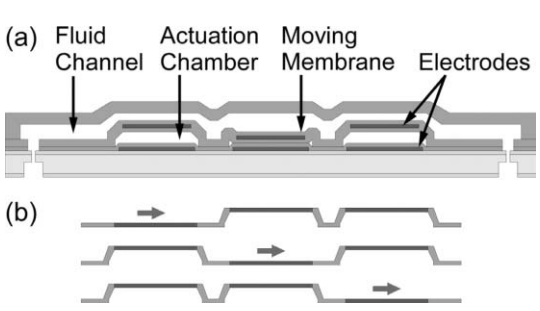

Fig. 1 Schematic of the micro pump design and operation. (a) Micro pump design. (As an example, the middle moving membrane is pulled down by electrostatic force). (b) 3-phase peristaltic sequence. Arrows indicate pumping direction.

Eqn. (1) is the basis on which we designed the physical dimensions of our pump. In choosing the parameters, many fabrication constraints have to be considered. For example, in order to achieve good electrical isolation around the electrodes, 1 μm parylene is necessary. Although thicker parylene improves the isolation, it also increases the membrane stiffness and results in more energy loss. For the composite moving membrane, two 1 μm thick parylene layers were chosen, and hence $t_m = 2$ μm. Also, $t_i = 2$ μm as there are two 1 μm insulation layers between the electrodes.

For safety and power consumption reasons, V_p should be minimized. A high actuation voltage also makes the pump prone to electrolysis because the fringing field can still leak into the fluid channel. Based on eqn. (1), to reduce the pull-in voltage, the height of the actuation gap d should be kept small, but a small actuation gap leads to a reduced volume expansion, which will cause the pumping rate to be small. Moreover, stiction becomes a serious problem when the gap between two surfaces is too small. We address this stiction problem in detail in a later section. Based on these considerations, d was chosen to be 3 μm in the design. Since V_p is inversely proportional to r, a larger membrane offers a lower V_p, but this larger membrane is also more easily affected by stiction. In the fabricated device, r was chosen to be 100 μm to limit V_p below 200 V. The fluid channel height h on top of the actuation membrane is related to compression/expansion ratio. While considering the capabilities of the sacrificial photoresist process, h was designed to be around 1 μm to maximize this ratio. Channels that are connected to the pump have a typical cross section of 100 μm (W) × 5 μm (H).

Fabrication

The fabrication process of the micro pump is shown in Fig. 2. Four layers of parylene were used as the structural material, photoresist and sputtered Si as the sacrificial materials, and chrome/gold as the electrode material. To start 1.5 μm thermal silicon oxide was grown on 4 inch silicon wafer. The backside oxide was patterned as a mask for DRIE etching. Inlets and outlets for the fluidic channels were then etched from the backside by DRIE using a standard Bosch process until a 50 μm thick silicon membrane was left. The main purpose of the inlet and outlet is to provide access to the pump for testing and characterization, so they are not an essential part of the pump. The process was continued on the front side. The front side oxide was patterned to expose the inlet and outlet for the fluidic channels that were formed later in the process. A Cr/Au (10 nm/300 nm) layer was thermally evaporated on the front side to form the bottom electrode. To isolate the bottom electrode from the environment, 1 μm parylene-C was deposited using room temperature chemical vapor deposition. Before parylene-C deposition, the adhesion promoter A-174 (SCS) was applied to the surface to ensure good adhesion between the parylene and the substrate. Next, a 300 nm sacrificial amorphous silicon layer was sputtered. The amorphous silicon was patterned using SF_6 chemistry and photoresist as the mask. On top of the amorphous silicon layer, the first photoresist sacrificial layer (4 μm thick) was formed and patterned. The combination of the amorphous silicon and the first photoresist sacrificial layer together defines the actuation gap. Next, the moving actuation diaphragm, consisting of a parylene/metal/parylene sandwich structure, was created. To do this, a second 1 μm thick parylene-C layer was deposited and patterned; the top electrode layer was formed by another evaporated Cr/Au

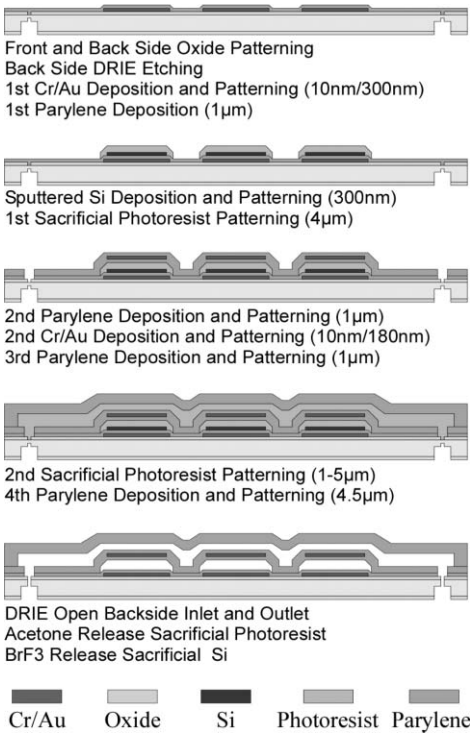

Fig. 2 Multilayer parylene technology used in the fabrication of the micro pump: 4 layers of parylene (structural); 2 layers of photoresist and 1 layer of sputtered Si (sacrificial); and 2 layers of Cr/Au (electrode).

layer (10 nm/180 nm); and a third 1 μm thick parylene-C layer was deposited to encapsulate the top electrode. This encapsulation insured that the electrode was isolated from the liquid-filled fluid channel. Patterning of the parylene was performed using oxygen plasma with photoresist as a mask. Once the moving membrane was finished, the fluid channel was formed by a second photoresist sacrificial layer and a 4.5 μm thick fourth parylene-C layer. The height of the fluid channel, as determined by the thickness of the second photoresist sacrificial layer, varied as a result of the uneven step coverage of photoresist over the existing structures. A partial double exposure was carefully performed to reduce the channel height immediately above the actuation chamber as required by the design specifications. Then, the remaining silicon membrane was etched away using DRIE to fully open the inlet and outlet of the fluid channel. Finally, the sacrificial photoresist was released using acetone. After releasing, the chips were rinsed with isopropanol and dried.

One important feature of this technology is that the whole process was carried out at low temperature once the silicon oxide was grown. All of the parylene and photoresist process steps were performed below 120 °C. Although exact temperatures during oxygen plasma etching, XeF_2 etching, and metallization were not measured, they were estimated to be <120 °C as well. This opens up the possibility of integrating electronics underneath the microfluidic network and performing post-CMOS surface micromachining. Fig. 3 is a photomicrograph of a fabricated micro pump.

Some process steps required special attention. To ensure sufficient adhesion of the parylene, before its deposition, either the adhesion promoter was used or several cleaning steps, such as a short period of O_2 plasma etching or a 5% HF dip for up to 30 s were performed. Also, for large membranes, stiction could happen during the drying process after the photoresist was dissolved away. To solve the stiction problem and produce a freestanding membrane, the remaining sputtered amorphous Si layer was etched away using gas phase XeF_2 or BrF_3 etching.[16]

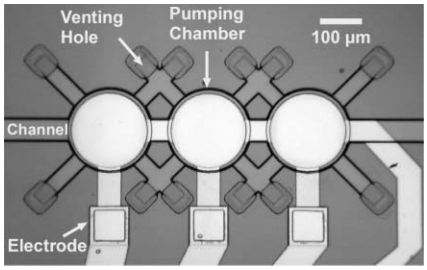

Fig. 3 Photomicrograph of a fabricated device. (Each pumping chamber is 200 μm in diameter. Venting holes are connected to the actuation chambers and separated from the fluid channel.)

Although a 4 μm sacrificial layer was used to compensate for any membrane deformation caused by stiction, the final actuation gap d was still less than the original design value.

Experimental

Electrostatic actuation

To test the electrostatic actuation of the moving membrane, a DC voltage was applied to the top electrode while the fixed electrode on the substrate was grounded. By varying the applied voltage and observing the actuation, the pull-in voltage can be determined. It was found that the pull-in voltage was typically around 110 V, but could vary from 80 V to 130 V between different chips. Large differences in pull-in voltage were observed especially between chips from different wafers. This variation in pull-in voltages was expected since pull-in is very sensitive to the actuation gap height d. Because stiction likely caused permanent deformation of the membrane, and since the degree of stiction can be affected by many factors (*e.g.* drying speed), final values of d were not well controlled. As suggested by eqn. (1), a 25% variation in d can change the pull-in voltage by a factor of 2. By comparing surface profile scans (WYKO NT1100, Veeco Instruments) of the actuation membrane before and after actuation, d was estimated to be around 2 μm. To calculate the theoretical pull-in voltage from eqn. (1), the residual stress s and the Young's modulus E were chosen to be 20 MPa and 3.2 GPa respectively. These values are based on a previous study[17] and the temperature history of the parylene membrane during the fabrication process. For a 100 μm radius and 2 μm thick parylene membrane with 2 μm actuation gap, the theoretical pull-in voltage is 126 V, which lies in the range of measured values.

If the membrane was actuated for extended durations or at high voltages (>200 V), shifts in the pull-in voltage were observed. In some cases, the membrane would remain in the actuated state even after the applied voltage was released. This type of behavior has been observed on other electrostatically actuated parylene structures studied by our group. Parasitic charging of dielectric surfaces was believed to be the main cause.[18,19] In addition to inconsistent actuation, electrolysis of the liquid in the channel was a serious problem as well. To reduce the extent of electrolysis and charging of the dielectric interface, an AC actuation signal was used.[19] For this study, a 5 kHz sinusoidal driving signal was used for the electrostatic actuation. The pull-in voltage using this AC signal was measured to be approximately 140 V_{peak} (100 V_{rms}). Even after extended periods of actuation, attenuation of the actuation magnitude was not observed.

Peristaltic actuation

3-phase peristaltic actuation was explored for the micro pump. For each actuation chamber, a control signal switched a solid-state relay that subsequently controlled the AC actuation voltage. Effectively, the control signal forms an envelope over

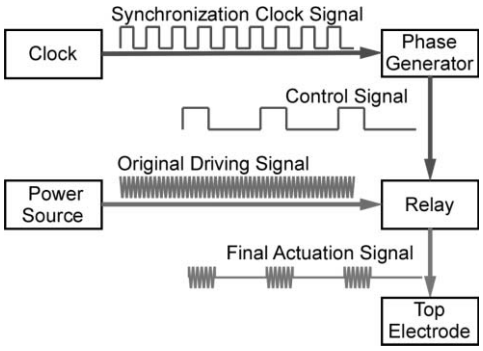

Fig. 4 Signals that were used to realize peristaltic actuation of the micro pump. Here the diagram shows all the signals used for one pumping chamber. The phase generator was a digital logic circuit that consists of 7400 series CMOS based ICs. The clock signal was given by a HP 33120A function generator. The relay was an optical isolation solid-state relay.

the driving signal, as shown in Fig. 4. This figure also shows that, to achieve peristaltic motion, the control signals of the three actuation chambers followed a 3-phase peristaltic sequence, which was generated by a logic circuit and driven by a 1–100 Hz clock. Fig. 5(a) shows the video snapshots of pump actuation during this 3-phase actuation sequence.

Pumping measurement

Flow rate measurement in the range of several nL min^{-1} proved to be very difficult. Any off-chip measurements would be extremely difficult due to the huge dead volume resulting from the packaging and coupling. For flow visualization, 1 μm polystyrene beads (Duke Scientific, Palo Alto, CA) were placed in the fluid at a concentration of tens of beads per nL. These beads allowed us to visually measure the pumping rate while not interfering with pump operation. To measure the pumping rate, first, video was recorded using the microscope of a probe station (Micromanipulator, Model 6000, Carson City, NV) and a CCD video camera (Hitachi, Model KP-D20BU). Then, by analyzing the video image of the moving beads, the flow rate could be deduced. During pumping, the beads were found to oscillate back and forth due to the pulse-like peristaltic actuation. It is the net movement that was translated into the calculated flow rate. This pump was tested with both ethanol and water. Ethanol proved to be a more reliable fluid for testing because even with an AC actuation signal, electrolysis of water still occurred in some cases. Fig. 5(b) shows sequential snapshots of a pumping test. The beads are highlighted in the photographs for clarity. The pump was actuated at 140 Vp (5 kHz AC), using a 20 Hz phase frequency for the 3-phase sequence. Here, phase frequency refers to the frequency of the entire 3-phase-cycle, which is 1/3 of the clock frequency. Bead velocity was measured to be $\sim$100 μm s^{-1}.

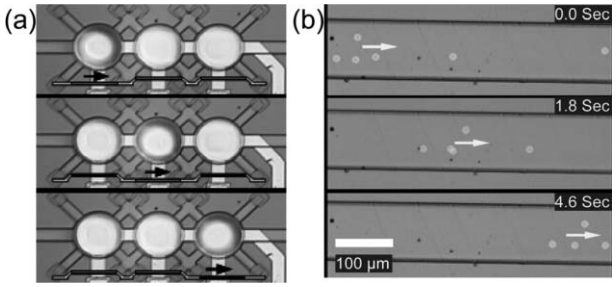

Fig. 5 Video snapshots. (a) Snapshots from 3-phase peristaltic actuation. Schematic view of the cross section was added to indicate the phase sequence. (b) Tracking of beads (highlighted for clarity) for flow rate measurement.

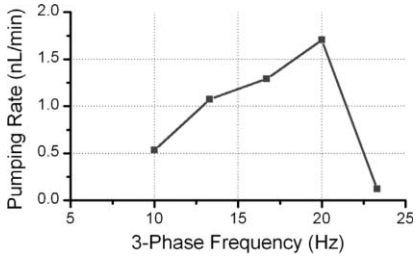

Fig. 6 Pumping rate *vs.* phase frequency. Here phase frequency refers to entire 3-phase-cycle frequency, which is 1/3 of clock frequency.

Fig. 6 shows the pumping rate of ethanol *vs.* phase frequency. The actuation voltage used in this test was again 140 Vp (5 kHz AC). The pumping rate reaches a maximum of 1.7 nL min^{-1} at 20 Hz and decreases at higher frequencies. It can be clearly seen that at lower frequencies the pumping rate increases almost linearly with the increasing frequency. At higher frequencies, the moving membrane is not fast enough to keep up with the actuation signal, so the actuation magnitude decreases, thus reducing the pumping efficiency. Due to the small pressures generated by this micro pump, we were not able to measure the pumping pressure directly using an off-chip pressure meter. The pumping pressure at the maximum flow rate (1.7 nL min^{-1}) was estimated to be 1.6 kPa. This pressure estimate was calculated by assuming that the channels connecting the pump to the inlet/outlet dominated the total flow resistance. The dimensions of these channels are 100 μm (W) $\times$ 5 μm (H) and have an equivalent length of 24 mm (L).

Modeling and analysis

To further understand the behaviour of the micro peristaltic pump, this section presents a model that considers the interactions of the vibrating membranes and the fluid flow. We first model each pumping chamber and the associated electrostatic membrane actuator, and then represent the pump as a system in which individual chambers and actuators interact with each other. The resulting lumped-parameter model will be solved numerically to yield insight into the peristaltic pump operation, especially the dependence of pumping flow rate on actuation frequency. Definitions of all the symbols used in this section are also listed in the Appendix.

As shown in Fig. 7, each pumping chamber is modelled as a thin fluid film sandwiched between a stationary rigid plate (representing the chamber ceiling) and a flexible membrane that is actuated by electrostatic force. At zero actuation voltage, the fluid film has thickness h while the air gap separating the membrane from the ground electrode has height d. As the pump operates at frequencies ($<$100 Hz) much lower than the membrane's natural frequency (estimated to be $\sim$600 kHz), the inertia of the membrane can be ignored. In addition, the membrane can be approximately represented by a rigid plate that is attached to an linear spring K and moves (quasistatically) with displacement δ. The effective spring constant is chosen in such a way that the pull-in voltage for a pair of

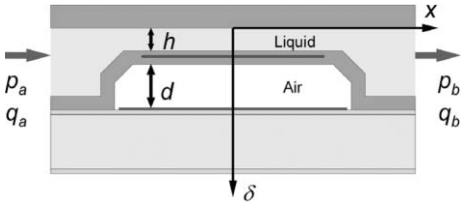

Fig. 7 Model for a pumping chamber.

parallel plates (one of which is spring-supported)[5,15] is consistent with eqn. (1). Thus,

$$K = \left(\frac{27}{8}\right)\left(\frac{1.55\pi}{\alpha}\right)\sigma t_{\mathrm{m}} = \left(\frac{16.43}{\alpha}\right)\sigma t_{\mathrm{m}} \tag{2}$$

As the membrane inertia is ignored, the forces on the membrane are in equilibrium:

$$K\delta = F_{\mathrm{h}} + F_{\mathrm{e}} \tag{3}$$

where the electrostatic actuation force F_{e} on the membrane due to an applied voltage V can be determined using the parallel-plate approximation, and is given by

$$F_{\mathrm{e}} = \frac{\varepsilon_0 V^2 A}{2(d + t_{\mathrm{i}}/\varepsilon_{\mathrm{p}} - \delta)^2} \tag{4}$$

To obtain a closed-form expression for the hydrodynamic force F_{h}, a first approximation is used where the fluid film, bounded by the pair of stationary and moving rigid plates as described above, is treated to be square in shape with area A. Improvements considering the circular shape of the fluid film are being addressed by ongoing work. As the liquid film thickness is small compared with the membrane diameter, and membrane vibrations occur at low frequencies (<100 Hz), it is reasonable to ignore fluid inertia and assume the pressure, p, to be uniform across the fluid film. The Reynolds equation in classical lubrication theory[20] then adequately describes the hydrodynamics of the liquid film. In the coordinate frame shown in Fig. 7, this equation takes the form

$$\begin{cases} \frac{\partial}{\partial x}\left((h+\delta)^3 \frac{\partial p}{\partial x}\right) = 12\mu\dot{\delta} \\ p|_{x=0} = p_{\mathrm{a}},\ p|_{x=\sqrt{A}} = p_{\mathrm{b}} \end{cases} \tag{5}$$

where μ is the liquid viscosity, and p_{a} and p_{b} are pressures immediately upstream and downstream of the chamber, respectively. The fluid pressure p, which is also the pressure on the membrane, can be found from this equation, and integrated to yield the hydrodynamic force as follows:

$$F_{\mathrm{h}} = -\frac{\mu A^2}{(h+\delta)^3}\dot{\delta} + \frac{1}{2}(p_{\mathrm{a}} + p_{\mathrm{b}})A \tag{6}$$

In addition, it can be shown that q_{a} and q_{b}, the rates of fluid flow into and out of the chamber, are related to the chamber inlet and outlet pressures by

$$q_{\mathrm{b}}^{\mathrm{a}} = \pm\frac{1}{2}\dot{\delta}A + \frac{(h+\delta)^3}{12\mu}(p_{\mathrm{a}} - p_{\mathrm{b}}) \tag{7}$$

The continuity of fluid flow also requires that

$$q_{\mathrm{a}} - q_{\mathrm{b}} = A\dot{\delta} \tag{8}$$

Thus, we have obtained a model for each pumping chamber, consisting of eqns. (3) (with eqns. (4) and (6) substituting for F_{e} and F_{h}), (7) and (8).

With the chamber model above, the pump can be represented as a system consisting of the three chambers and the inlet and outlet channels leading to and from the pump, as illustrated in Fig. 8. Here, the deflection δ_{i} of the ith membrane (actuated by voltage V_{i}), is related to the flow rates q_{i} and $q_{\mathrm{i+1}}$, and pressures p_{i} and $p_{\mathrm{i+1}}$ by eqns. (3), (4) and (6). Neglecting flow inertia, the inlet and outlet channels are each represented by a flow resistance given by

$$R_{\mathrm{L}} = \frac{12\mu L}{WH^3} \tag{9}$$

where L, W, and H are the channel length, width and height,

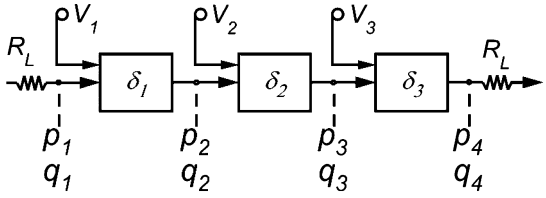

Fig. 8 Representation of the pump as a system consisting of individual chambers and load microchannels.

respectively. Then, assuming the reservoirs where the channels originate or terminate are at atmospheric pressure, the flow rate and pressures immediately upstream and downstream of the pump are related by

$$-p_1 = R_{\mathrm{L}}q_1,\ p_4 = R_L q_4 \tag{10}$$

The pump model hence consists of a system of nonlinear ordinary differential equations as the electrostatic and hydrodynamic forces (eqns. (4) and (6)), and the chamber flow rates (eqns. (7) and (8)) are nonlinear in membrane deflections, but can be readily solved numerically. Here we used the commercial numerical simulation software MATLAB (The Mathworks Inc., Natick, MA).

We now present pumping flow rates and pressures calculated from the pump model. Consistent with the experiment, a 3-phase voltage sequence is used:

$$V_{\mathrm{i}} = V(t - (i-1)T/3)\ i = 1,2,3 \tag{11}$$

Here $V(t)$ is a square wave of period T, such that $V(t) = 140$ V if $0 < t < T/3$, and $V(t) = 0$ V if $T/3 < t < T$. We choose nominal values $d = 2$ μm, and allow h to vary from 0.1 to 1.2 μm. The inlet and outlet channels each have effective length 24 mm, width 100 μm, and height 5 μm. The time-averaged pumping flow rate and pressure difference $p_4 - p_1$ (Fig. 8) obtained for various values of h are shown in Fig. 9 and Fig. 10. It can be seen that in general, for a given fluid film thickness h, the average flow rate and pressure difference initially increase with frequency, reaches a maximum (*i.e.* resonance), and then decrease with frequency. In particular, for $h = 0.6$ μm, the average flow rate achieves a maximum of 1.78 nL min^{-1}, and the average pressure difference achieves a maximum of 1.63 kPa, both at 18 Hz. This behavior is consistent with the experimental data (Fig. 6). Note that $h = 0.6$ μm, along with $d = 2$ μm, is considered to lie in the range of the actual parameter values for the device tested, which we were not able to accurately measure. It can also be seen from the

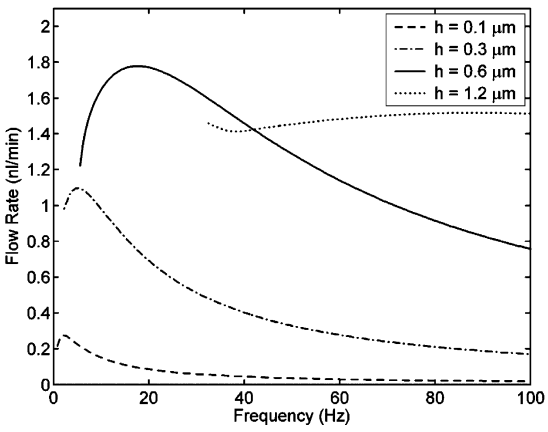

Fig. 9 Calculated frequency dependence of the time-averaged pumping flow rate.

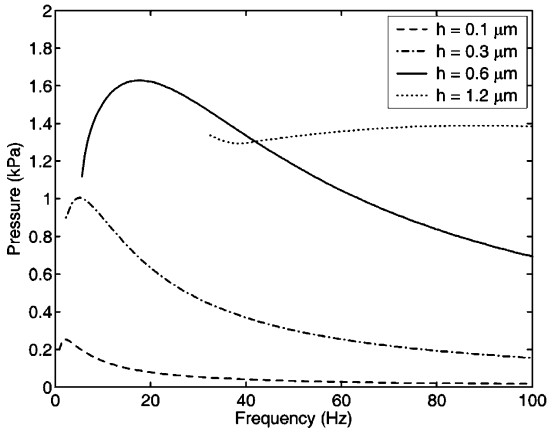

Fig. 10 Calculated frequency dependence of the time-averaged pressure difference $p_4 - p_1$.

figures that as h decreases, the frequency at which the flow rate and pressure reach the maximum steadily decreases, due to increasingly larger damping of membrane vibrations (eqn. (6)). The maximum flow rate and pressure difference initially increase, and then decrease with h. This is due to the competing effects, both resulting from the decrease in h, of increased damping on membrane vibrations, and reduced backward flow due to improved sealing of the fluid chambers.

In Fig. 9 and Fig. 10, the actuation voltage (140 V) exceeds the pull-in voltage (126 V), and the membranes therefore vibrate beyond the critical displacement $(d+t_i/\varepsilon_p)/3$ as given by static theory.[5] The vibration is adequately described by our model provided the excitation frequency is not too low to cause the touchdown of the membrane on the bottom electrode. Therefore, computations have been performed for each h only at frequencies that do not cause membrane touchdown. The frequency dependence of the flow rate can be attributed to the complex interplay of the excitation frequency, and the amplitude and phase of membrane stroke vibrations. For example, as shown in Fig. 9 and Fig. 10, there is a local minimum in flow rate and pressure for $h = 1.2$ μm, although this minimum is quite insignificant. More importantly, the interplay between the frequency and membrane stroke volume is the cause for the flow rate to reach the maximum (Fig. 9). At low frequencies the tendency for an increase in frequency to increase the flow rate dominates over the tendency for the reduced membrane stroke volume to decrease the flow rate, and at frequencies beyond the maximum, the relative significance of these tendencies is reversed.

Conclusions

Based on a multilayer parylene, surface-micromachining technology, an electrostatically actuated micro peristaltic pump has been developed. The electrostatic actuation of parylene structures was studied along with the problems associated with it, such as charging and electrolysis. An AC actuation voltage combined with a 3-phase peristaltic actuation sequence, were used to demonstrate fluid pumping. A flow rate of 1.7 nL min^{-1} and an estimated pumping pressure of 1.6 kPa were achieved. The relationship between pumping and phase frequency was also characterized. The pump dynamics and performance were then investigated further by an analysis based on a lumped-parameter model of the system. The analysis correctly predicted the trend in the experimental data. Due to the pump's small footprint, large-scale integration becomes feasible. Moreover, since the micro pump shares the same platform technology as many other devices we have previously developed (*e.g.* valves, electrospray ionization nozzles, filters and flow sensors), total integration for a μTAS becomes feasible.

Appendix

All symbols used in the paper are listed in Table 1 below.

Symbols used in the paper.

Definition	Symbol (Value)
Constants or material properties	
Permittivity of free space	ε_0
Viscosity of liquid (water or ethanol)	μ
Dielectric constant of parylene	ε_p (3.1)
Density of parylene	ρ (1.3 g cm^{-3})
Residual stress of parylene membrane	σ (20 MPa)
Young's modulus of parylene	E (3.2 GPa)
Poisson's ratio of parylene	v (0.4)
Model parameters	
Thickness of actuation membrane	t_m (2 μm)
Thickness of insulation layer	t_i (2 μm)
Radius of actuation membrane	r (100 μm)
Height of actuation gap	d (3 μm)
Thickness of fluid film on top	h (1 μm)
Effective mass of plate (membrane)	M
Effective stiffness of plate (membrane)	K
Area of membrane	A
Pumping load	R_L
Height of load channel	H (5 μm)
Width of load channel	W (100 μm)
Length of load channel	L (24 mm)
Electrostatic pull-in voltage	V_p (110 V)
Applied voltage	V or V_i
Plate displacement	δ or δ_i
Electrostatic force on membrane	F_e
Hydrodynamic force	F_h
Pressure up/downstream of chamber	$p_{a,b}$ or p_i
Flow rate in/out of chamber	$q_{a,b}$ or q_i
Time	t
Period of entire 3-phase cycle	T

Acknowledgements

This work is supported in part by NSF CNSE Engineering Research Center at Caltech (EEC-9402726), NIH (5R01 RR06217-10), and DARPA (Bioflips Program, N66001-00-C-8092) grants awarded to Caltech, and by an NSF (CTS-0304568) grant awarded to Carnegie Mellon.

References

1 P. R. Selvaganapathy, E. T. Carlen and C. H. Mastrangelo, Recent progress in microfluidic devices for nucleic acid and antibody assays, *Proc. IEEE*, 2003, **91**, 954–975.
2 N. Lion, T. C. Rohner, L. Dayon, I. L. Arnaud, E. Damoc, N. Youhnovski, Z. Y. Wu, C. Roussel, J. Josserand, H. Jensen, J. S. Rossier, M. Przbylski and H. H. Girault, Microfluidic systems in proteomics, *Electrophoresis*, 2003, **24**, 3533–3562.
3 N. T. Nguyen, X. Y. Huang and T. K. Chuan, MEMS-micropumps: A review, *J. Fluids Eng.*, 2002, **124**, 384–392.
4 L. X. Chen, J. P. Ma, F. Tan and Y. F. Guan, Generating high-pressure sub-microliter flow rate in packed microchannel by electroosmotic force: potential application in microfluidic systems, *Sens. Actuators, B*, 2003, **88**, 260–265.
5 G. T. A. Kovacs, *Micromachined Transducers Sourcebook*, WCB/McGraw-Hill, Boston, MA, 1998.
6 C. Cabuz, E. I. Cabuz, W. R. Herb, T. Rolfer and D. Zook, Mesoscopic sampler based on 3D array of electrostatically

activated diaphragms, *The 10th International Conference on Solid-State Sensors, Actuators and Microsystems, (Transducers'99)*, 1999.
7 J. W. Judy, T. Tamagawa and D. L. Polla, Surface-machined micromechanical membrane pump, *Proceedings of IEEE International Workshop on Micro Electro Mechanical Systems (MEMS '91)*, 1991.
8 M. Q. Bu, T. Melvin, G. Ensell, J. S. Wilkinson and A. G. R. Evans, Design and theoretical evaluation of a novel microfluidic device to be used for PCR, *J. Micromech. Microeng.*, 2003, **13**, S125–S130.
9 R. Zengerle and M. Richter, Simulation of microfluid systems, *J. Micromech. Microeng.*, 1994, **4**, 192–204.
10 M. Carmona, S. Marco, J. Samitier and J. R. Morante, Dynamic simulations of micropumps, *J. Micromech. Microeng.*, 1996, **6**, 128–130.
11 X.-Q. Wang and Y.-C. Tai, A normally closed in-channel micro check valve, *The 13th Annual International Conference on Micro Electro Mechanical Systems (MEMS 2000)*, 2000.
12 M. A. Unger, H. P. Chou, T. Thorsen, A. Scherer and S. R. Quake, Monolithic microfabricated valves and pumps by multilayer soft lithography, *Science*, 2000, **288**, 113–116.
13 T. Thorsen, S. J. Maerkl and S. R. Quake, Microfluidic large-scale integration, *Science*, 2002, **298**, 580–584.
14 C. Grosjean, X. Yang and Y.-C. Tai, A thermopneumatic peristaltic micropump, *The 10th International Conference on Solid-State Sensors, Actuators and Microsystems, (Transducers'99)*, 1999.
15 P. M. Osterberg and S. D. Senturia, M-TEST: A test chip for MEMS material property measurement using electrostatically actuated test structures, *J. Microelectromech. Syst.*, 1997, **6**, 107–118.
16 T. J. Yao, X. Yang and Y. C. Tai, BrF3 dry release technology for large freestanding parylene microstructures and electrostatic actuators, *Sens. Actuators, A*, 2002, **97–8**, 771–775.
17 T. A. Harder, T.-J. Yao, Q. He, C.-Y. Shih and Y.-C. Tai, Residual stress in thin-film parylene-C, *The 15th IEEE International Conference on Micro Electro Mechanical Systems (MEMS 2002)*, 2002, Las Vegas, NV.
18 T.-J. Yao, K. Walsh and Y.-C. Tai Dielectric charging effects on Parylene electrostatic actuators, *The 15th IEEE International Conference on Micro Electro Mechanical Systems (MEMS 2002)*, 2002, Las Vegas, NV.
19 W. van der Wijngaart, H. Ask, P. Enoksson and G. Stemme, A high-stoke, high-pressure electrostatic actuator for valve applications, *Sens. Actuators, A*, 2002, **100**, 264–271.
20 A. Cameron and C. M. M. Ettles, *Basic Lubrication Theory*, E. Horwood, Halsted Press, Chichester, 1981.